Multitask quantum thermal machines and cooperative effects

Jincheng Lu,[1] Zi Wang,[2] Rongqian Wang,[3] Jiebin Peng,[4] Chen Wang,[5,*] and Jian-Hua Jiang[3,†]

[1]*Jiangsu Key Laboratory of Micro and Nano Heat Fluid Flow Technology and Energy Application, School of Physical Science and Technology, Suzhou University of Science and Technology, Suzhou 215009, China*

[2]*Center for Phononics and Thermal Energy Science, China-EU Joint Lab on Nanophononics, Shanghai Key Laboratory of Special Artificial Microstructure Materials and Technology, School of Physics Science and Engineering, Tongji University, Shanghai 200092, China*

[3]*Institute of Theoretical and Applied Physics & School of Physical Science and Technology & Collaborative Innovation Center of Suzhou Nano Science and Technology, Soochow University, Suzhou 215006, China*

[4]*School of Physics and Optoelectronic Engineering, Guangdong University of Technology, Guangzhou 510006, Guangdong Province, China*

[5]*Department of Physics, Zhejiang Normal University, Jinhua, Zhejiang 321004, China*

(Received 18 September 2022; revised 22 December 2022; accepted 10 February 2023; published 21 February 2023)

Including the phonon-assisted inelastic process in thermoelectric devices makes it possible to enhance the performance of nonequilibrium work extraction. In this work, we demonstrate that inelastic phonon-thermoelectric devices have a fertile functionality diagram, where particle current and phononic heat currents are coupled and fueled by the chemical potential difference. Such devices can simultaneously perform multiple tasks, e.g., heat engines, refrigerators, and heat pumps. Guided by the entropy production, we mainly study the efficiencies and coefficients of performance of multitask quantum thermal machines, where the roles of the inelastic scattering process and multiple biases in multiterminal setups are emphasized. Specifically, in a three-terminal double-quantum-dot setup with a tunable gate, we show that it efficiently performs two useful tasks due to the phonon-assisted inelastic process. For the four-terminal four-quantum-dot thermoelectric setup, we find that additional thermodynamic affinity furnishes the system with both enriched functionality and enhanced efficiency. Our work provides insights into optimizing phonon-thermoelectric devices.

DOI: 10.1103/PhysRevB.107.075428

I. INTRODUCTION

Understanding the performance of thermoelectric transport at the nanoscale is of significant importance for its potential applications in quantum technology [1–5]. Much effort has been devoted to achieving high efficiency and a coefficient of performance in thermoelectric nanodevices both theoretically [6–8] and experimentally [9–24], which mainly originate from elastic transport processes [25,26]. Interestingly, Mahan and Sofo proposed the "best thermoelectrics" by using conductors with very narrow energy bands to reduce the thermal conductivity based on the Wiedemann-Franz law [27]. However, it was recently discovered that phonon thermal transport will inevitably suppress the figure or merit and output power in the zero bandwidth limit [28]. The carrier of particlea and heat current for the elastic transport processes is electrons, so it is impossible to spatially separate them. In contrast, it may be possible to realize such a separation of heat and charge currents in inelastic transport processes [29].

Recently, another fundamental category, i.e., inelastic transport processes, was explored [30–36]. One exciting perspective is that the inclusion of an additional terminal to "decouple" the particle and heat currents may significantly improve thermoelectric efficiency. Until now, a vast number of valuable works have been carried out to study inelastic transport in thermoelectric systems, e.g., Coulomb-coupled quantum dot (QD) systems [16,37,38], metal-superconductor junctions [39], and boson-assisted thermoelectric devices [40–42]. However, the study of multiterminal energy conversion and transfer is still in its infancy. In such energy conversion and transfer, the thermodynamic machine usually performs a single task, such as a refrigerator [12,14,43–45], a heat pump [46–48], or a heat engine [21,22,49–52]. Intriguingly, as proposed by Entin-Wohlman *et al.* [53] and Manzano *et al.* [54], a three-terminal device is considered to be a hybrid thermal machine that performs multiple efficient tasks simultaneously by introducing a reference temperature. Consequently, the thermoelectric effect accompanied by one electric current and two heat currents is analyzed.

In this work we provide a universal efficiency based on the concept of entropy production [55]. We show that inelastic thermoelectric devices with multiple electric currents and/or multiple heat currents can be nominated as hybrid thermal machines, i.e., devices concurrently performing multiple useful tasks [54,56]. Specifically, we desire to analyze different thermoelectric devices performing distinct tasks, e.g., heat engines, refrigerators, and heat pumps. When a system connects to "N" reservoirs, the entropy production rate of the whole system is described as $\dot{S}_{\rm tot} = \sum_{i=1}^{N} \dot{S}^i$, where $\dot{S}^i = -I_Q^i/T_i$ is the entropy production rate of the ith reservoir [57], with I_Q^i being the heat current out of the ith reservoir. Moreover, the

*Corresponding author: wangchen@zjnu.cn
†jianhuajiang@suda.edu.cn

particle and energy conservations result in $\sum_{i=1}^{N} I_p^i = 0$ and $\sum_{i=1}^{N} I_E^i = 0$, with I_v^i $(v = p, E)$ being the particle (energy) current flowing out from the ith reservoir into the system. Then, we select the rth reservoir as the reference reservoir, which is characterized as a reference temperature T_r and one chemical potential μ_r associated with the electron particle number N_e^r. Straightforwardly, the rth particle and energy currents can be obtained as $I_p^r = -\sum_{i\neq r}^{N} I_p^i$ and $I_E^r = -\sum_{i\neq r}^{N} I_E^i$. Considering the expression of the heat current from the rth reservoir, i.e., $I_Q^r = I_E^r - \mu_r I_p^r$, it can be reexpressed as $I_Q^r = -\mu_r I_p^r - \sum_{i\neq r}^{N}(I_Q^i + \mu_i I_p^i)$. Therefore, the rate of total entropy production is given by

$$T_r \dot{S}_{\rm tot} = T_r \sum_{i=1}^{N} \dot{S}^i = \sum_{i=1}^{N} \sum_{v=p,Q} I_v^i A_v^i, \tag{1}$$

where A_v^i is the affinity, which can be the electrochemical potential difference or temperature gradient, e.g., $A_p^i = \mu_i - \mu_r$, and $A_Q^i = (T_i - T_r)/T_i$. Here we need to point out that if the heat reservoir is the phononic one, there is no electrochemical potential difference, i.e., $A_p^i \equiv 0$. Then, the efficiency is defined as the ratio of all the entropy decrease terms (the useful rates) to all the entropy increase terms (the wasteful rates) [54,58–60]

$$\phi = -\frac{\sum_i \sum_{v=p,Q}^{-} I_v^i A_v^i}{\sum_i \sum_{v=p,Q}^{+} I_v^i A_v^i} \leqslant 1, \tag{2}$$

where $\sum_i \sum_{v=p,Q}^{\pm} I_v^i A_v^i$ denotes the sum over the positive and negative terms of the entropy production rates, respectively. According to the second law of thermodynamics, the efficiency is bounded via $\phi \leqslant 1$ [61].

We should note that such efficiency in Eq. (2) can be alternatively derived by including the concept of the generalized free energy as proposed in Ref. [54], which is based on the choice of the reference reservoir. Specifically, the rate of free energy of the ith reservoir $\dot{\mathcal{A}}_i$ is expressed as $-\dot{\mathcal{A}}_i = (\dot{E}_i - \mu \dot{I}_p^i) + T_r \dot{S}_i$. Combined with the energy relation $\dot{E}_i = \dot{I}_Q^i + \mu_i \dot{I}_p^i$, the rate of total free energy can be reexpressed as $-\dot{\mathcal{A}}_{\rm tot} = \sum_i (\mu_i - \mu_r) I_p^i + \sum_i \frac{(T_i - T_r)}{T_i} I_Q^i$, which actually has the identical form to $T_r \dot{S}_{\rm tot}$. Therefore, it is expected to obtain such efficiency.

It is known that typical kinds of efficiency have been studied in both the equilibrium and nonequilibrium regimes [54,59,62,63]. Interestingly, with the two-terminal setup the relation between efficiency ϕ and conventional efficiency $\eta = W/Q$ (W and Q are the output work and input heat) can be obtained as [62]

$$\phi = \eta/\eta_C, \tag{3}$$

where $\eta_C = 1 - T_c/T_h$ is the Carnot efficiency, and T_c and T_h are the temperatures of the cold and hot reservoirs, respectively. Equation (2) is general for distinct functional machines, including a heat engine, a refrigerator, and a heat pump. Note that Eq. (3) is applicable to a heat engine. One key mission in quantum thermodynamics is to find out the optimal efficiency and the corresponding maximal power of thermal machines.

While considering energy conversion, thermoelectric cooperative effects have been demonstrated to be an effectual way to improve conversion efficiency (figure of merit) [62]. As shown in Fig. 1, the thermal machine connects to two input currents and one output current, and there are two thermoelectric effects associated with different chemical potentials and/or temperature gradients. The essence of cooperative effect is to modulate the input currents through regulating the thermodynamic affinities. For instance, there is only one input current in mode I and mode II, while mode III has two input currents. It is found that the efficiency of mode III can be greater than that of modes I and II, i.e., $\max(\phi_{\rm III}) \geqslant \max(\phi_{\rm I}, \phi_{\rm II})$.

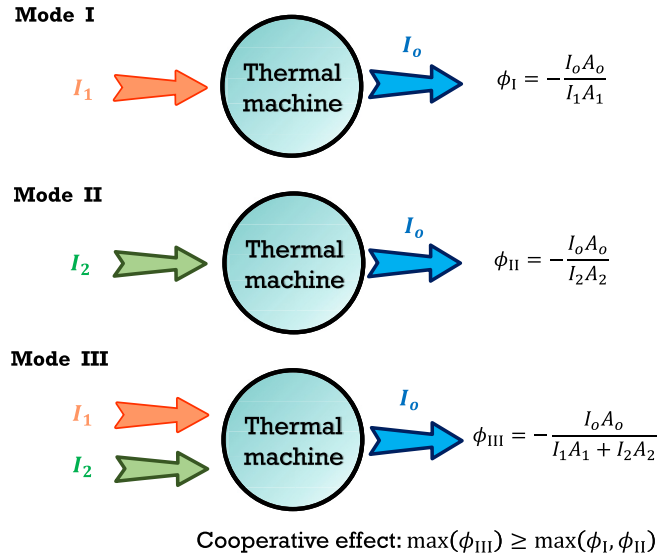

FIG. 1. Schematic illustration of thermoelectric cooperative effects in a quantum thermal machine. I_i $(i = 1, 2)$ denotes the input current, I_o is the output current, and A_i is the corresponding affinity. ϕ_i $(i = \rm I, II, II)$ is the efficiency of the thermal machine.

Here we primarily examine the general theoretical framework of multiterminal devices, i.e., a double-QD three-terminal system comprising two electronic terminals and a phonon bath (Sec. II), and four-QD four-terminal system (Sec. III), define the particle and heat currents and the corresponding thermodynamic driving forces, and they use those quantities to reexpress the efficiencies of the thermal machine for different tasks. We also discuss thermodynamic multitasks of the various setups in the linear response, based on the Onsager formalism. Finally, Sec. IV is devoted to the conclusions. Throughout this work, we set electron charge $e \equiv 1$ and Planck constant $\hbar \equiv 1$.

II. THE THREE-TERMINAL DOUBLE-QD DEVICE

In this section, we will present a generic inelastic transport model to illustrate multitasks of hybrid thermal machines. The simplest nontrivial geometry configuration for inelastic transport is the three-terminal system, where energy absorbed/emitted by the electron is assisted by a third phonon bath, differing from the left reservoir and the right reservoir. This model is characterized as a hopping double-QD model [42,51,64–66]. At the linear thermoelectric response regime, one remarkable feature of double QDs is that the three-terminal system exhibits a large thermopower and a

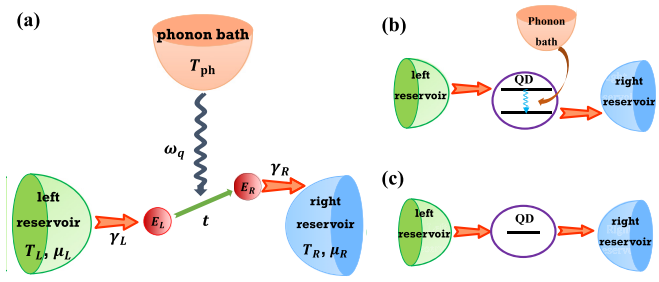

FIG. 2. Illustration of a three-terminal double-QD system. An electron that leaves the left reservoir into the left QD (with energy E_L) hops to the right QD (with energy E_R) as assisted by a phonon from the phonon bath (with temperature $T_{\rm ph}$). The electron then tunnels into the right reservoir from the right QD. The electrochemical potential and the temperature of the left reservoir (right reservoir) are μ_L and T_L (μ_R and T_R), respectively. $\gamma_{L/R}$ are the hybridization energies of the QDs to the left/right reservoir, respectively. Also shown is an illustration of (b) inelastic and (c) elastic thermoelectric transport.

high figure of merit [40]. Moreover, it is found that nonlinear thermoelectric transport can further enhance energy efficiency and output power under nonlinear driving sources [51]. Here, we mainly focus on the efficiencies and coefficients of performance of a multitask three-terminal inelastic phonon-thermoelectric device.

A. The basic setup and currents

The three-terminal double-QD device consists of the left reservoir, the right reservoir, and a phonon bath, as schematically depicted in Fig. 2. The QDs are labeled by L and R with tunable energy levels E_L and E_R. Here we select the case $E_R > E_L$. An electron leaves the left QD and hops to the right QD, which is simultaneously assisted by one phonon from the phonon bath (with temperature $T_{\rm ph}$). The Hamiltonian of the double-QD device is

$$\hat{H} = \hat{H}_{\rm DQD} + \hat{H}_{e\text{-ph}} + \hat{H}_{\rm lead} + \hat{H}_{\rm tun} + \hat{H}_{\rm ph}, \tag{4}$$

with

$$\hat{H}_{\rm DQD} = \sum_{i=L,R} E_i \hat{b}_i^\dagger \hat{b}_i + t(\hat{b}_L^\dagger \hat{b}_R + \text{H.c.}), \tag{5a}$$

$$\hat{H}_{e\text{-ph}} = \sum_q \lambda_q \hat{b}_L^\dagger \hat{b}_R (\hat{d}_q + \hat{d}_q^\dagger) + \text{H.c.}, \tag{5b}$$

$$\hat{H}_{\rm ph} = \sum_q \omega_q \hat{d}_q^\dagger \hat{d}_q, \tag{5c}$$

$$\hat{H}_{\rm lead} = \sum_{j=L,R} \sum_k \varepsilon_{j,k} \hat{b}_{j,k}^\dagger \hat{b}_{j,k}, \tag{5d}$$

$$\hat{H}_{\rm tun} = \sum_k V_{L,k} \hat{b}_L^\dagger \hat{b}_{L,k} + \sum_k V_{R,k} \hat{b}_R^\dagger \hat{b}_{R,k} + \text{H.c.}, \tag{5e}$$

where $\hat{b}_i^\dagger$ ($\hat{b}_i$) is the creation (annihilation) operator of an electron in the i QD, and E_i is the QD energy, t is the tunneling between the two QDs, $\gamma_{L(R)} = 2\pi \sum_k |V_{L(R),k}|^2 \delta(E - \varepsilon_{L(R),k})$ is the coupling between the QD and the left (right) reservoir, λ_q is the strength of electron-phonon interaction, and $\hat{d}_q^\dagger$ ($\hat{d}_q$) is the creation (annihilation) operator of a phonon with the frequency ω_q.

There are particle I_p^i ($i = L, R$), energy I_E^i ($i = L, R$, ph), and heat I_Q^i ($i = L, R$, ph) currents out of the ith reservoir, which are denoted by gray lines with arrows in Fig. 2(a) [30,41]. Accordingly, the electric and phononic heat currents are given by $I_Q^i = I_E^i - \mu_i I_p^i$ ($i = L, R$) and $I_Q^{\rm ph} = I_E^{\rm ph}$. We show that the current I_i is positive when flowing towards the hybrid quantum system. Moreover, energy conservation leads to the relation $I_E^L + I_E^R + I_Q^{\rm ph} = 0$ [30], while particle conservation results in $I_p^L + I_p^R = 0$. Moreover, the entropy production relation of the system is given by [67] $-\dot{S}_{\rm tot} = I_Q^L/T_L + I_Q^R/T_R + I_Q^{\rm ph}/T_{\rm ph}$. Combining the particle and energy current conservation relations, the entropy production rate can be reexpressed as

$$T_L \frac{dS_{\rm tot}}{dt} = I_p^R A_p^R + I_Q^R A_Q^R + I_Q^{\rm ph} A_Q^{\rm ph}, \tag{6}$$

where $A_p^R = \mu_R - \mu_L$, $A_Q^R = 1 - \frac{T_L}{T_R}$, and $A_Q^{\rm ph} = 1 - \frac{T_L}{T_{\rm ph}}$.

We make the approximation that the elastic (el) current between reservoirs (that involve coherent tunneling from dot L to dot R via the t-term in $H_{\rm DQD}$) can be treated independently from the inelastic (inel) current from dot L to dot R (that involve absorbing or creating a phonon in the phonon bath). We calculate the elastic current by assuming no inelastic hopping from dot L to dot R, whereas we calculate the inelastic currents by assuming no elastic hopping from dot L to dot R. Then we sum these two terms to obtain the total current,

$$I = I^{\rm el} + I^{\rm inel}. \tag{7}$$

Based on the Fermi golden rule [40,68], the inelastic transition rates between two quantum dots are described as

$$\Gamma_{L\to R} \equiv \gamma_{e\text{-ph}} f_L (1 - f_R) N_p^-, \tag{8a}$$

$$\Gamma_{R\to L} \equiv \gamma_{e\text{-ph}} f_R (1 - f_L) N_p^+, \tag{8b}$$

where $f_{L(R)}$ is the occupation of the $L(R)$ dot, $N_p^\pm = N_B + \frac{1}{2} \pm \frac{1}{2}\text{sgn}(E_R - E_L)$ with $N_B \equiv [\exp(|E_R - E_L|/T_{\rm ph}) - 1]^{-1}$ being the Bose-Einstein distribution for phonons, and the spectral function of the phononic reservoir is given by $\gamma_{e\text{-ph}} = 2\pi \sum_q |\lambda_q|^2 \delta(E - \omega_q)$, which is selected to be constant. Then, we assume that the dot-electronic reservoir coupling strengths are much larger than the dot-phononic reservoir one, i.e., $\gamma_{L(R)} \gg \gamma_{e\text{-ph}}$, where the steady-state distributions of two QDs can be approximated by the distribution of local electronic reservoirs. Consequently, we obtain $f_i \approx \{\exp[(E_i - \mu_i)/k_B T_i] + 1\}^{-1}$, where f_i ($i = L, R$) is the Fermi-Dirac distribution function of the ith electronic reservoir. Hence, one is able to obtain the contribution of inelastic processes to the heat currents,

$$I_Q^{L,\rm inel} = (E_L - \mu_L) I_p^{L,\rm inel}, \tag{9a}$$

$$I_Q^{R,\rm inel} = -(E_R - \mu_R) I_p^{L,\rm inel}, \tag{9b}$$

$$I_Q^{\rm ph,inel} = (E_R - E_L) I_p^{L,\rm inel}, \tag{9c}$$

where $I_p^{L,\rm inel} = \Gamma_{L\to R} - \Gamma_{R\to L}$. In Fig. 2(b), we can see that the inelastic process mainly results from the electron-phonon

interaction processes, which involve collaborative transport between three reservoirs.

In contrast, the electron-phonon scattering process does not contribute to elastic current [see Fig. 2(c)], which only involves the electron transmission processes. If we consider the weak tunneling between two dots ($t \ll |E_R - E_L|$), the elastic currents may be approximated via the noninteracting version of the Landauer-Büttiker formula [69,70],

$$\begin{aligned} I_e^{L,\mathrm{el}} &= \int \frac{dE}{2\pi}\mathcal{T}(E)[f_L(E) - f_R(E)], \\ I_Q^{L,\mathrm{el}} &= \int \frac{dE}{2\pi}(E-\mu_L)\mathcal{T}(E)[f_L(E) - f_R(E)], \\ I_Q^{\mathrm{ph,el}} &= 0, \end{aligned} \tag{10}$$

where the energy-dependent transmission function can be obtained via the Caroli formula [67] $\mathcal{T}(E) = \mathrm{Tr}[\hat{G}^r(E)\hat{\Gamma}_L\hat{G}^a(E)\hat{\Gamma}_R]$. Specifically, two Green functions are approximated as $\hat{G}^r(E) = [\hat{G}^a(E)]^\dagger = \begin{pmatrix} E-E_L+i\gamma_L/2 & -t \\ -t & E-E_R+i\gamma_R/2 \end{pmatrix}^{-1}$ (see the details in Appendix A), and the two transition functions defined as $\langle v|\hat{\Gamma}_u|v'\rangle = \gamma_u\delta_{u,v}\delta_{u,v'}$ $(u, v, v' = L, R)$ are given by $\hat{\Gamma}_L = \begin{pmatrix} \gamma_L & 0 \\ 0 & 0 \end{pmatrix}$ and $\hat{\Gamma}_R = \begin{pmatrix} 0 & 0 \\ 0 & \gamma_R \end{pmatrix}$. Thus, the transmission function can be obtained as

$$\mathcal{T}(E) = \frac{t^2\gamma_L\gamma_R}{\left|\left(E-E_L+\frac{i\gamma_L}{2}\right)\left(E-E_R+\frac{i\gamma_R}{2}\right)-t^2\right|^2}. \tag{11}$$

Note that elastic processes do not contribute to the heat current I_Q^{ph}. Finally, the total nonequilibrium current, both contributed by elastic and inelastic processes, is expressed as $I = I^{\mathrm{el}} + I^{\mathrm{inel}}$.

Then the power produced by the reservoirs for the device is expressed as [30,53]

$$\dot{W} = I_p^R\Delta\mu, \tag{12}$$

where $\Delta\mu = \mu_R - \mu_L \equiv A_p^R$ is the chemical potential difference. By default, we will consider the temperatures as $T_R < T_L < T_{\mathrm{ph}}$, where the temperature of the left reservoir is chosen as the reference temperature. Hence, it should be easier to characterize which task the system is performing.

B. The efficiency of power production, cooling, and heating by performing a single task

In this part, we introduce the efficiencies for three thermodynamic operations: heat engines, refrigerators, and heat pumps. The efficiency is a dimensionless ratio where the device's output drives its input. For example, heat engines convert temperature gradients to extract useful work, e.g., a thermoelectric engine [71]. In such a thermoelectric heat engine, the heat current absorbed from the hot reservoir (phonon bath) is used to drive particle current against the chemical potential bias $\Delta\mu$, i.e., $I_Q^R < 0$, $I_Q^{\mathrm{ph}} > 0$, and $\dot{W} < 0$. According to Eq. (2), the efficiency of the thermoelectric heat engine is given by

$$\phi_{\mathrm{E}} = \frac{-\dot{W}}{I_Q^R A_Q^R + I_Q^{\mathrm{ph}} A_Q^{\mathrm{ph}}}. \tag{13}$$

Based on the above relation ($\phi_{\mathrm{E}} > 0$), we know that the negative entropy production associated with power produced by the reservoirs, $\dot{W} < 0$, is compensated by the positive entropy production of $I_Q^R A_Q^R + I_Q^{\mathrm{ph}} A_Q^{\mathrm{ph}}$, in agreement with Kedem and Caplan [72].

For the refrigerator operation, the negative entropy production occurs when heat current flows out of the coldest reservoir ($I_Q^R > 0$), but no other useful task is performed (i.e., $I_Q^{\mathrm{ph}} > 0$ and $\dot{W} > 0$). Such efficiency is also termed the coefficient of performance, defined as

$$\phi_{\mathrm{R}} = \frac{-I_Q^R A_Q^R}{I_Q^{\mathrm{ph}} A_Q^{\mathrm{ph}} + \dot{W}}. \tag{14}$$

The third type of thermal operations is the heat pump, which is characterized as heat current flowing into the hot reservoir ($I_Q^{\mathrm{ph}} < 0$), but no other useful task being performed ($I_Q^R < 0$ and $\dot{W} > 0$). For the heat pump, we obtain [73]

$$\phi_{\mathrm{P}} = \frac{-I_Q^{\mathrm{ph}} A_Q^{\mathrm{ph}}}{I_Q^R A_Q^R + \dot{W}}. \tag{15}$$

From the above discussion, we know that if we ignore the inelastic scattering processes, the heat current involved with the phonon bath becomes vanishing. The whole entropy production is simplified to $T_L\frac{dS_{\mathrm{tot}}^{\mathrm{el}}}{dt} = I_p^{R,\mathrm{el}}A_p^R + I_Q^{R,\mathrm{el}}A_Q^R$. And the three-terminal setup is reduced to the two-terminal one.

When multiple terminals cooperate with each other, the thermal machine may perform multiple useful tasks simultaneously, e.g., the third terminal is either a phononic or an electronic reservoir (see Appendix C). However, the two terminal setups are also able to perform two tasks simultaneously: cooling one reservoir necessarily comes together with pumping heat in the other one.

C. The performance of the hybrid thermal machine for multiple tasks

We will show that the three-terminal configuration is sufficient to perform nontrivial multiple thermodynamic tasks [54]. First, work can be used to cool down the cold reservoir and warm up the hot reservoir (i.e., $I_Q^R > 0$, $I_Q^{\mathrm{ph}} < 0$, and $\dot{W} > 0$). Hence, the device simultaneously acts as a refrigerator and a heat pump. Specifically, using Eq. (2), the efficiency in this operation regime reads

$$\phi_{\mathrm{PR}} = \frac{-I_Q^R A_Q^R - I_Q^{\mathrm{ph}} A_Q^{\mathrm{ph}}}{\dot{W}}, \tag{16}$$

where the subscript stands for *pump-refrigerator*. The efficiency for producing work and cooling the cold reservoir (i.e., $I_Q^R > 0$, $I_Q^{\mathrm{ph}} > 0$, and $\dot{W} < 0$) is given by

$$\phi_{\mathrm{ER}} = \frac{-I_Q^R A_Q^R - \dot{W}}{I_Q^{\mathrm{ph}} A_Q^{\mathrm{ph}}}, \tag{17}$$

while for the heat engine and heat pump (i.e., $I_Q^R < 0$, $I_Q^{\mathrm{ph}} < 0$, and $\dot{W} < 0$), the corresponding efficiency is expressed as

$$\phi_{\mathrm{EP}} = \frac{-I_Q^{\mathrm{ph}} A_Q^{\mathrm{ph}} - \dot{W}}{I_Q^R A_Q^R}. \tag{18}$$

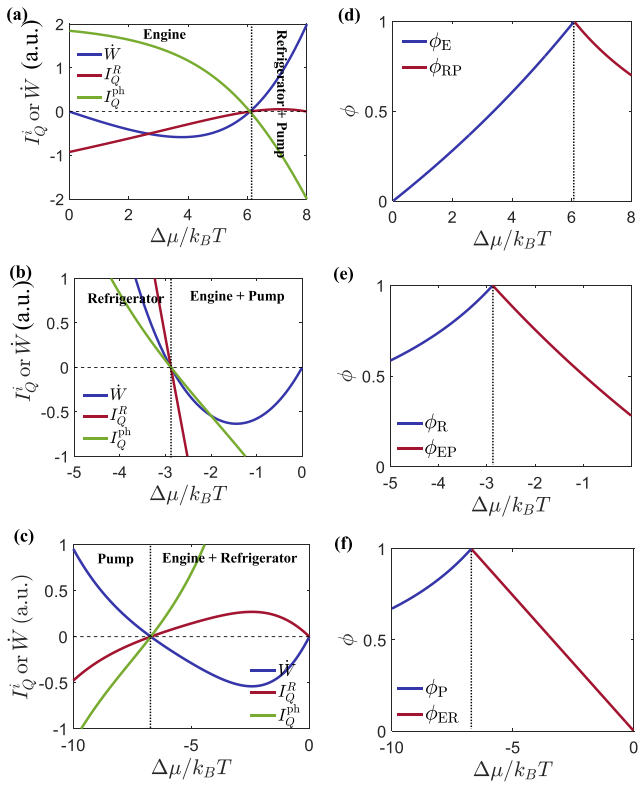

FIG. 3. Three-terminal double-QD system performance. (a)–(c) Currents and power, and (d)–(f) efficiencies as a function of the chemical potential difference $\Delta\mu$ for simultaneous heating, cooling, and power production, where (a) and (d) $E_L = 4k_BT$, $E_R = -4k_BT$; (b) and (e) $E_L = 12k_BT$, $E_R = 10k_BT$; and (c) and (f) $E_L = -12k_BT$, $E_R = 0$. The other parameters are $t = 0.15k_BT$, $\gamma_l = \gamma_r = 0.4k_BT$, $\gamma_{e\text{-ph}} = 0.1k_BT$, $k_BT_R = k_BT$, $k_BT_{\rm ph} = 5.0k_BT$, $k_BT_L = 1.5k_BT$, and $k_BT = 10$ meV.

From the definitions in Eqs. (13)–(18), it is clear that the efficiency better characterizes the function of a thermal machine compared with conventional thermodynamic efficiency. Moreover, we should point out that the system is unable to simultaneously heat the hottest reservoir, cool the coldest reservoir, and produce work, which stems from the constraint imposed by the Second Law of Thermodynamics, i.e., $\phi \leqslant 1$ [61].

The versatility of this setup is manifested in Fig. 3. In particular, we consider the possibility of reproducing hybrid configurations, e.g., engine-pump, engine-refrigerator, and refrigerator-pump. We include two separate contributions associated with two different tasks being performed simultaneously. Here we show how heat currents/output work [Figs. 3(a)–3(c)] as well as the corresponding efficiencies [Figs. 3(d)–3(f)] characterize thermodynamic multitasks with respect to the chemical potential difference $\Delta\mu$ [74]. Through varying $\Delta\mu$, we find that the operation switches between a hybrid regime and the complementary single-task regime. Based on Eqs. (9) and (10), the corresponding vanishing position for currents, termed the current cutoff voltage, can be obtained as $I_p^R \approx 0$. For example, in Fig. 3(d) we see that when $0 < \Delta\mu < 6k_BT$, the device produces power to the reservoirs, which performs the task of being a heat engine $\dot{W} > 0$ (see the blue line). As $\Delta\mu > 6k_BT$, the device will heat the hottest reservoir $I_Q^{\rm ph} < 0$ and cool the coldest reservoir $I_Q^R > 0$, which acts as hybrid thermal machines. In analogy, we see a similar behavior in Figs. 3(e) and 3(f). When $\Delta\mu \approx -3k_BT$ $(-7k_BT)$, the device will change from a single task of a refrigerator (heat pump) to two simultaneous tasks of heat engine and heat pump (engine and refrigerator).

We also note that thermodynamic laws set a bound on the efficiency of the quantum thermal machine, where the output work and efficiency cannot be maximized simultaneously. Such a restriction refers to the power-efficiency tradeoff [25,62,75–78], e.g., the operating efficiency reaching the unit and the output work vanishing. In addition to the above functions, our three-terminal setups characterized as Eq. (14) can also be designed for cooling by heating processes. As proposed by Cleuren *et al.* [41], the chemical potential difference is kept at zero, and the coolest electronic reservoir is cooled by the hot phonon bath.

In the above, we focus on the thermoelectric energy conversion efficiency of the three-terminal multitask thermal machines. We note that in the linear-response regime, the thermoelectric effects have been demonstrated as an effective way to lead to the enhancement of heat engine performance in our previous works [79,80]. In Appendix B, we briefly discuss how the thermoelectric cooperative effects may not only improve the performance of the heat engine, but they may also be applicable for refrigerators, heat pumps, and even for multitask thermal machines.

III. THE FOUR-TERMINAL THERMOELECTRIC QD SYSTEMS

To further illustrate the functionality of inelastic hybrid thermal machines, we consider another typical thermoelectric transport model, i.e., four-terminal thermoelectric QD systems [81–91]. In Ref. [92], we studied an unconventional inelastic thermoelectric effect, referred to as cooling by the transverse heat current effect. It describes the cooling process of the source driven by the heat exchange between two thermal baths, rather than total heat injected into the central quantum system [41]. In this section, we study how to use the temperature gradient to overcome the chemical potential, which is different from generating useful work (heat engines), or to use the chemical potential against the temperature bias to generate the heat current from the hot reservoir to the cold one (refrigerators and/or heat pumps). Interestingly, this device performs multiple useful tasks simultaneously, which demonstrates that more thermodynamic affinities enrich the implementation of hybrid operations.

The mesoscopic four-terminal thermoelectric devices coupled with two electric reservoirs and two phononic reservoirs are depicted in Fig. 4(a). The system consists of four QDs: QD 1 and QD 2 with energies E_1 and E_2 in the upper channel are coupled with the hot phononic reservoir H, while QD 3 and QD 4 with energies E_3 and E_4 in the lower channel are connected with the cold phononic bath C. The inelastic-scattering processes dominate the thermoelectric transport [93]. I_p^i (i=L, R) is the particle current flowing from the reservoir i into the system, and I_Q^i ($i = L, R, H, C$) is the heat current that flows from the reservoir i into the system.

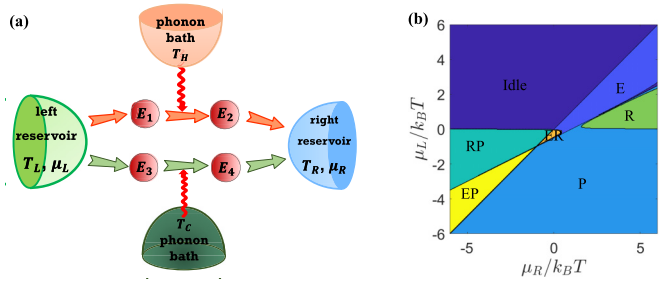

FIG. 4. (a) Schematic of four-terminal four-QD thermoelectric systems. The left and right reservoirs with chemical potentials $\mu_{L/R}$ and temperatures $T_{L/R}$ connect with the central QD systems, in which there are two parallel transport channels: the upper channel has two QDs (with energies E_1 and E_2) and a phonon bath H (with temperature T_H); the lower channel has two QDs (with energies E_3 and E_4) and a phonon bath C (with temperature T_C). The two channels are spatially separated so that the phonon bath H (C) couples only to the upper (lower) channel. (b) Map of the system functionality as functions of the chemical potentials μ_L and μ_R. The parameters are $E_1 = 2.0k_BT$, $E_2 = 0$, $E_3 = 1.0k_BT$, $E_4 = 5.0k_BT$, $\gamma_{e\text{-ph}} = 0.1k_BT$, $k_BT_L = k_BT$, $k_BT_C = 0.7k_BT$, $k_BT_H = 2.0k_BT$, $k_BT_R = 0.5k_BT$, and $k_BT = 10$ meV.

Due to energy conservation ($I_Q^L + \mu_L I_p^L + I_Q^H + I_Q^C + I_Q^R + \mu_R I_p^R = 0$) and particle conversation ($I_p^L + I_p^R = 0$), the entropy production rate of the whole system is given by [92]

$$T_L \frac{dS}{dt} = I_p^R A_p^R + I_Q^R A_Q^R + I_Q^H A_Q^H + I_Q^C A_Q^C, \tag{19}$$

where the affinities are defined as $A_p^R = \mu_R - \mu_L$, $A_Q^R = 1 - \frac{T_L}{T_R}$, $A_Q^H = 1 - \frac{T_L}{T_H}$, and $A_Q^C = 1 - \frac{T_L}{T_C}$. The Lth reservoir is considered to be the reference reservoir. Here, we restrict our discussion to having only one energy level in each QD. In this setup, the phonon-assisted particle currents through two independent upper and lower channels are described as [66]

$$I_{\text{up}} = \Gamma_{1\to 2} - \Gamma_{2\to 1}, \quad I_{\text{down}} = \Gamma_{3\to 4} - \Gamma_{4\to 3}, \tag{20}$$

where $\Gamma_{i\to j}$ is the electron tunneling rate from QD i to QD j [92]. Then, the particle and heat currents derived from the Fermi golden rule [94] can be written as

$$\begin{aligned} &I_p^L = I_{\text{up}} + I_{\text{down}}, \quad I_Q^L = (E_1 - \mu_L)I_{\text{up}} + (E_3 - \mu_L)I_{\text{down}}, \\ &I_Q^R = -(E_2 - \mu_R)I_{\text{up}} - (E_4 - \mu_R)I_{\text{down}}, \\ &I_Q^H = (E_2 - E_1)I_{\text{up}}, \quad I_Q^C = (E_4 - E_3)I_{\text{down}}. \end{aligned} \tag{21}$$

The output power of the device $-\dot{W}$ is given by

$$\dot{W} = I_p^R \Delta\mu, \tag{22}$$

where $\Delta\mu = \mu_R - \mu_L \equiv X_p^R$ is the chemical potential difference. In this four-terminal system, we specifically set the temperatures as

$$T_R < T_C < T_L < T_H. \tag{23}$$

The definitions of efficiency for the four-terminal device in different operation regimes are shown in Table I. It should be noted that distinct selection of the reference quantities (i.e., T_r and μ_r) may result in different specific behaviors of the efficiency. Usually, one would select a single typical kind of reference arrangements to analyze the multitasking of this quantum thermal machine. If one changes the reference reservoir, the specific working features of the thermal machine may vary.

If we specify the Lth reservoir as the reference reservoir and consider the situation $\mu_R = \mu_L$ and $T_C = (2/T_L - 1/T_H)^{-1}$, we find that the efficiency of refrigerators is simplified as $\phi = -(2I_Q^R)/(I_Q^H - I_Q^C)$, as done in Ref. [92]. Then, we enter one working mode of cooling by the transverse heat current effect, i.e., the coldest Rth reservoir can be cooled by passing a heat current between the H phonon bath and the C phonon bath. In such cooling by the transverse heat current effect, there is no need to inject heat into the quantum system, for the driving force of this process is the energy exchange between the two phononic reservoirs mediated by the central quantum system. Moreover, one should maintain a high temperature in the phonon reservoir to efficiently realize cooling by the heat current operation [92]. However, if we consider the

TABLE I. Functionality of a four-terminal four-QD thermal machine.

Thermal progresses	Work and heat currents	Efficiency
Heat engine	$I_Q^R < 0, I_Q^H > 0, \dot{W} < 0, I_Q^C < 0$	$\phi_{\text{E}} = \frac{-\dot{W}}{I_Q^R A_Q^R + I_Q^C A_Q^C + I_Q^H A_Q^H}$
Heat pump	$I_Q^H < 0, I_Q^R < 0, \dot{W} > 0, I_Q^C < 0$	$\phi_{\text{P}} = \frac{-I_Q^H A_Q^H}{I_Q^R A_Q^R + I_Q^C A_Q^C + \dot{W}}$
Refrigerator	$I_Q^R > 0, I_Q^H > 0, \dot{W} > 0, I_Q^C < 0$	$\phi_{\text{R}} = \frac{-I_Q^R A_Q^R}{I_Q^H A_Q^H + I_Q^C A_Q^C + \dot{W}}$
Refrigerator and heat pump	$I_Q^R > 0, I_Q^H < 0, \dot{W} > 0, I_Q^C < 0$	$\phi_{\text{PR}} = \frac{-I_Q^R A_Q^R - I_Q^H A_Q^H}{I_Q^C A_Q^C + \dot{W}}$
Engine and refrigerator	$I_Q^R > 0, I_Q^H > 0, \dot{W} < 0, I_Q^C < 0$	$\phi_{\text{ER}} = \frac{-I_Q^R A_Q^R - \dot{W}}{I_Q^C A_Q^C + I_Q^H A_Q^H}$
Engine and heat pump	$I_Q^R < 0, I_Q^H < 0, \dot{W} < 0, I_Q^C < 0$	$\phi_{\text{EP}} = \frac{-I_Q^H A_Q^H - \dot{W}}{I_Q^C A_Q^C + I_Q^R A_Q^R}$

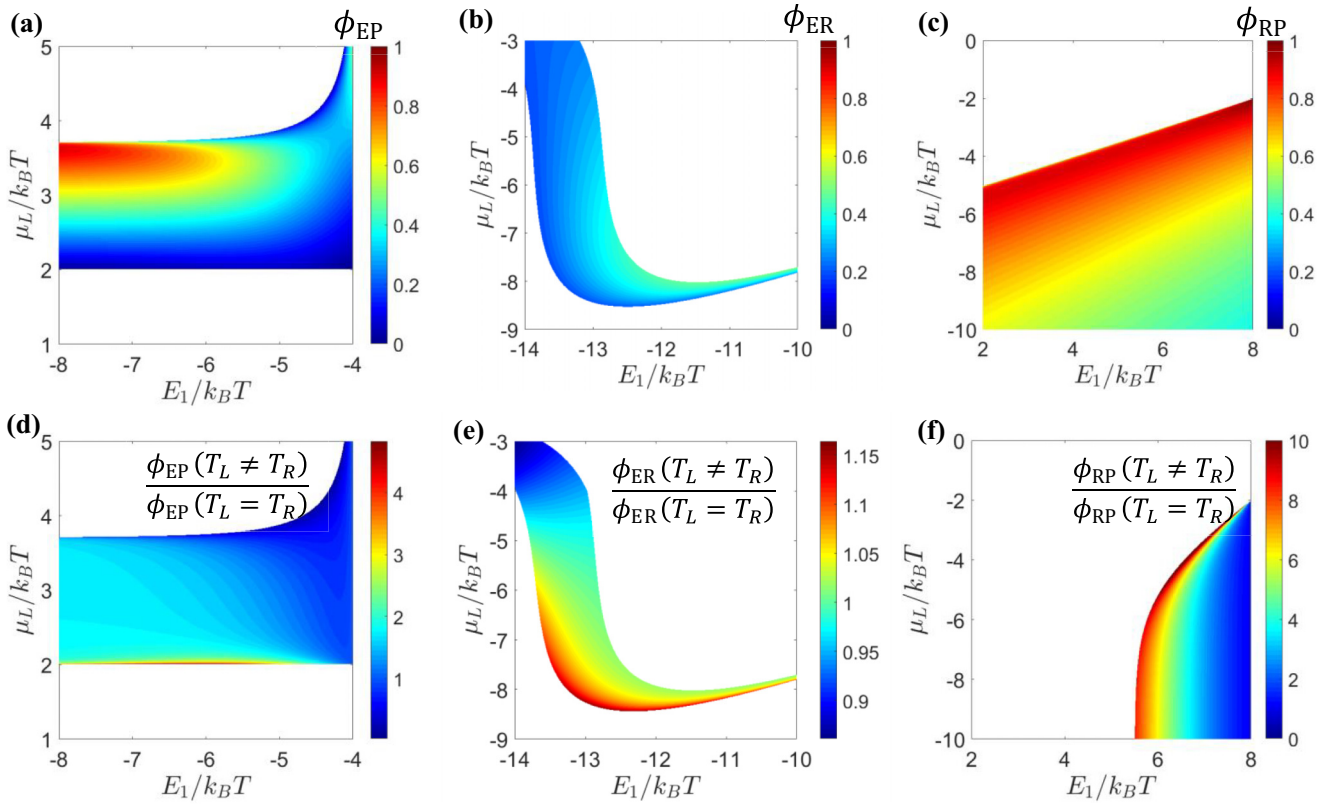

FIG. 5. The efficiencies of hybrid thermal machines (a) $\phi_{\rm EP}$, (b) $\phi_{\rm ER}$, and (c) $\phi_{\rm RP}$ as functions of the chemical potential μ_L and QD energy E_1 for $T_C = 0.7k_BT$. (d)–(f) Comparing the efficiency for the $T_L \neq T_C$ case and $T_L = T_C$ as functions of the chemical potential μ_L and QD energy E_1. The parameters are (a) and (d) $E_2 = -4.0k_BT$, $E_3 = 2.0k_BT$, $E_4 = -1.0k_BT$; (b) and (e) $E_2 = 6.0k_BT$, $E_3 = 6.0k_BT$, $E_4 = 8.0k_BT$; (c) and (f) $E_2 = 8.0k_BT$, $E_3 = 6.0k_BT$, $E_4 = -4.0k_BT$. The other parameters are $\gamma_{e\text{-ph}} = 0.1k_BT$, $k_BT_L = k_BT$, $k_BT_H = 2.0k_BT$, $k_BT_R = 0.5k_BT$, and $k_BT = 10$ meV. The white region indicates that the function of the hybrid thermal machines is not performed.

cooling process driven by voltage bias, the cooling mechanism from the transverse heat current effect breaks down, which may also result in efficient cooling behavior.

Figure 4(b) displays all possible functionalities for the thermal machines, and the change of current symbol means the realization of different functions by tuning the chemical potential of the left (μ_L) and right (μ_R) reservoirs. From this map figure, we observe that the four-terminal device can realize any functions and perform different tasks by adjusting physical parameters.

To emphasize the role of thermodynamic biases in the four-terminal system, we compare the performance of such a setup at $T_L = T_R$ with the case $T_L \neq T_R$ for the same three-terminal quantum-dot thermal machines in Fig. 5. We first show the efficiency of the thermal machines in Figs. 5(a)–5(c), which exhibit two useful tasks as functions of QD energy E_1 and chemical potential μ_L, and the efficiency can even reach unity in some parameter regions. In Figs. 5(d)–5(f) we compare the above two cases, and it is easy to find that the maximum efficiency can be significantly improved when the four-terminal device goes from the condition of $T_L = T_R$ to $T_L \neq T_R$. Through concrete numerical results, we find that the setup with multiple biases can substantially enlarge the parameter region of the high efficiency, and thus provide a promising pathway toward high-performance thermal machines.

Finally, we point out that there are three Seebeck coefficients induced by three temperature gradients, which originate from the three thermal affinities A_Q^R, A_Q^H, and A_Q^C in the linear-response regime for the four-terminal thermoelectric device. Correspondingly, the figures of merit refer to the conventional longitudinal thermoelectric effects and the unconventional transverse thermoelectric effects, respectively.

IV. CONCLUSIONS

In this work, a general thermodynamic efficiency was defined from an entropic point of view, which can characterize the functions of the thermal machines, such as heat engine, refrigerator, and heat pump, without the need to specifically define a reference temperature. The efficiency is appointed for each functionality as the ratio of the output (the consumed usable energy) to the consumed (the target heat).

We discussed the thermodynamic operations of a phonon-thermoelectric device that performs multiple useful tasks simultaneously in two typical thermoelectric systems [(i) devices with two electronic terminals and a phonon terminal, and (ii) those with two electronic terminals and two phononic terminals], where phonon-assisted inelastic processes dominate the transport. In the three-terminal device, we found the parameter region and the corresponding efficiency of the thermal machines for power production, cooling, heating, and

the simultaneous combinations. It is found that a hybrid thermal machine can be realized only if inelastic processes are taken into account. In the four-terminal device, in addition to demonstrating that the device can perform two useful tasks, we further emphasized the improvement of efficiency by multiple thermodynamic biases.

Finally, it should be pointed out that our study is based on steady-state transport. The performance of a periodically driven thermoelectric device with inelastic transport undertaking multitasks will be a fascinating topic for future study.

ACKNOWLEDGMENTS

We thank the anonymous reviewers for their valuable comments on the revision of the manuscript. We are grateful to Jie Ren for many interesting discussions. This work was supported by the funding for the National Natural Science Foundation of China under Grants No. 12125504, No. 12074281, and No. 11704093, the Opening Project of Shanghai Key Laboratory of Special Artificial Microstructure Materials and Technology, and Jiangsu Key Disciplines of the Fourteenth Five-Year Plan (Grant No. 2021135).

APPENDIX A: ELECTRON GREEN'S FUNCTION

In this Appendix, we give expressions for different components of the noninteracting electronic Green's functions in a frequency domain. We write

$$\hat{G}^{r/a} = (E\hat{\mathrm{I}} - \hat{H}_{\mathrm{DQD}} + \hat{\Sigma}^{r/a})^{-1},$$
$$\hat{G}^{</>} = \hat{G}^{r}\hat{\Sigma}^{</>}\hat{G}^{a}, \tag{A1}$$

where $\hat{H}_{\mathrm{DQD}}$ is the Hamiltonian of the double-QDs system,

$$\hat{H}_{\mathrm{DQD}} = \begin{pmatrix} E_L & t \\ t & E_R \end{pmatrix}, \tag{A2}$$

and $\hat{\Sigma}^{r/a}(E)$ are different components of the self-energy, which is additive in the left L and right R electronic reservoirs, i.e., $\hat{\Sigma}^{r/a/</>}(E) = \hat{\Sigma}_L^{r/a/</>}(E) + \hat{\Sigma}_R^{r/a/</>}(E)$. Here considering the noninteracting approximation, we obtain $\hat{\Sigma}_L^{r/a}(E) = \left(\begin{smallmatrix} \mp i\gamma_L/2 & 0 \\ 0 & 0 \end{smallmatrix}\right)$, $\hat{\Sigma}_L^{<}(E) = \left(\begin{smallmatrix} if_L(E)\gamma_L & 0 \\ 0 & 0 \end{smallmatrix}\right)$, and $\hat{\Sigma}_L^{>}(E) = \left(\begin{smallmatrix} -i[1-f_L(E)]\gamma_L & 0 \\ 0 & 0 \end{smallmatrix}\right)$. Similar expressions hold for the right electronic reservoir self-energy, with $L \to R$. From the above, the noninteracting electronic Green's function is written as

$$\hat{G}^{r}(E) = [\hat{G}^{a}(E)]^{\dagger} = \begin{pmatrix} E - E_L + i\gamma_L/2 & -t \\ -t & E - E_R + i\gamma_R/2 \end{pmatrix}^{-1}. \tag{A3}$$

APPENDIX B: LINEAR TRANSPORT AND THERMOELECTRIC COOPERATIVE EFFECT

In the linear-response regime, the performance of a thermal machine can be characterized by two main parameters, namely the figure of merit ξ and the power factor P. In Refs. [79,80], we demonstrated that two coexisting thermoelectric effects, i.e., the longitudinal thermoelectric effect and the transverse one, can generate cooperative effects, which leads to an enhancement of the heat engine performance. Here, we further demonstrate that the thermoelectric cooperative effects may be a general theory. In principle, it can not only improve the performance of a quantum heat engine, but it can also be applicable for refrigerators, heat pumps, and even for multitask thermal machines.

Based on Eqs. (9) and (10), the transport equations are reexpressed as [40]

$$\begin{pmatrix} I_p^R \\ I_Q^R \\ I_Q^{\mathrm{ph}} \end{pmatrix} = \begin{pmatrix} M_{11} & M_{12} & M_{13} \\ M_{12} & M_{22} & M_{23} \\ M_{13} & M_{23} & M_{33} \end{pmatrix} \begin{pmatrix} A_p^R \\ A_Q^R \\ A_Q^{\mathrm{ph}} \end{pmatrix}, \tag{B1}$$

where the Onsager coefficients $M_{ij} = M_{ij}^{\mathrm{el}} + M_{ij}^{\mathrm{inel}}$ include both the elastic and inelastic transport components [94]. Moreover, the second law of thermodynamics, i.e., $dS/dt \geqslant 0$ [70], leads to

$$M_{11}, M_{22}, M_{33} \geqslant 0, \quad M_{11}M_{22} \geqslant M_{12}^2,$$
$$M_{11}M_{33} \geqslant M_{13}^2, \quad M_{22}M_{33} \geqslant M_{23}^2, \tag{B2}$$

and the determinant of the transport matrix in Eq. (B1) should be non-negative.

For systems with time-reversal symmetry, the maximal efficiency and the maximal power of the three-terminal devices are expressed as

$$\phi_{\max} = \frac{\sqrt{\xi+1}-1}{\sqrt{\xi+1}+1}, \quad W_{\max} = \frac{1}{4}PT^2, \tag{B3}$$

where ξ is the dimensionless figure of merit, and P is the power factor of quantum thermal machines, respectively. Equation (B3) is a general expression, and it is independent of the function being performed by the thermal machine. The maximal efficiency quantifies the performance of hybrid thermal machines, including heat engines, refrigerators, heat pumps, and combinations thereof. Clearly, $\phi_{\max}$ approaches the unit when ξ approaches ∞.

Alternatively from the geometric perspective, the two temperatures can be parametrized as [95]

$$A_Q^R = T_A\cos\theta, \quad A_Q^{\mathrm{ph}} = T_A\sin\theta. \tag{B4}$$

Consequently, the figure of merit and the power factor are described as

$$\frac{1}{\xi(\theta)} = \frac{M_{22}\cos^2\theta + 2M_{23}\sin\theta\cos\theta + M_{33}\sin^2\theta}{M_{11}(S_1\cos\theta + S_2\sin\theta)^2} - 1, \tag{B5}$$

$$P(\theta) = M_{11}(S_1\cos\theta + S_2\sin\theta)^2, \tag{B6}$$

where $S_1 = M_{12}/M_{11}$ and $S_2 = M_{13}/M_{11}$ denote the longitudinal and transverse thermopowers, respectively. Using

TABLE II. Longitudinal and transverse thermoelectric effects and their maximum.

Performance	Figure of merit	Power factor
Longitudinal	$\xi_L = \frac{M_{11}S_1^2}{M_{22}-M_{11}S_1^2}$	$P_L = M_{11}S_1^2$
Transverse	$\xi_T = \frac{M_{11}S_2^2}{M_{33}-M_{11}S_2^2}$	$P_T = M_{11}S_2^2$
Maximum	$\xi_{\max} = \frac{M_{33}M_{12}^2 - 2M_{12}M_{13}M_{23} + M_{22}M_{13}^2}{\mathcal{M}}$	$P_{\max} = M_{11}(S_1^2+S_2^2)$

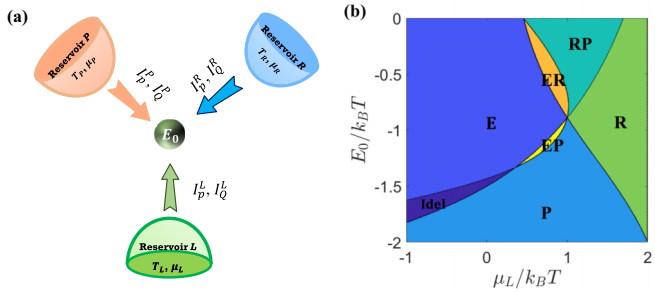

FIG. 6. (a) Schematic figure of a three-terminal single-QD thermoelectric device. The QD with a single energy level E_0 is connected in series to three fermionic reservoirs i ($i = L, R, P$). The chemical potential and the temperature of the reservoirs are μ_i and T_i, respectively. The constant Γ represents the coupling between the QD and the reservoir. (b) Map of the system efficiency as functions of the chemical potential μ_L and QD energy E_0. The parameters are $\mu_R = 0$, $\mu_P = 2.0k_BT$.

Eqs. (B5) and (B6), it is straightforward to obtain the expressions of the longitudinal ($\theta = 0$ or π) and transverse ($\theta = \pi/2, 3\pi/2$) figure of merit and power factor. The details can be found in Table II, where $\mathcal{M} = M_{11}M_{22}M_{33} - M_{11}M_{23}^2 - M_{33}M_{12}^2 + 2M_{12}M_{13}M_{23} - M_{22}M_{13}^2$. Interestingly, we find that $\xi_{\max} \geqslant \max(\xi_L, \xi_T)$ and $P_{\max} \geqslant \max(P_L, P_T)$. Such results are irrelevant with respect to the specific working mode of the multitask thermal machine. Hence, we may expect that the efficiency could be improved by exploiting cooperative effects once the thermoelectric figure of merit is enhanced.

APPENDIX C: THE HYBRID THERMAL MACHINES: THREE-TERMINAL SINGLE-LEVEL QD SYSTEM

In this Appendix, we study the operation and performance of the elastic thermoelectric devices that perform multiple useful tasks simultaneously. In our construction [see Fig. 6(a)], a single QD system exchanges particle and energy with three electronic reservoirs, L, R, and P. The particle and heat currents flowing from the reservoir into the system are expressed as [67]

$$I_p^L = \sum_{i=R,P} \frac{\Gamma_i\Gamma_L[f_L(E_0) - f_i(E_0)]}{\Gamma_L + \Gamma_i}, \tag{C1a}$$

$$I_p^R = \sum_{i=L,P} \frac{\Gamma_i\Gamma_R[f_R(E_0) - f_i(E_0)]}{\Gamma_R + \Gamma_i}, \tag{C1b}$$

$$I_p^P = \sum_{i=L,R} \frac{\Gamma_i\Gamma_P[f_P(E_0) - f_i(E_0)]}{\Gamma_P + \Gamma_i}, \tag{C1c}$$

and

$$I_Q^L = \sum_{i=R,P} \frac{(E_0 - \mu_L)\Gamma_i\Gamma_L[f_L(E_0) - f_i(E_0)]}{\Gamma_L + \Gamma_i}, \tag{C2a}$$

$$I_Q^R = \sum_{i=L,P} \frac{(E_0 - \mu_R)\Gamma_i\Gamma_R[f_R(E_0) - f_i(E_0)]}{\Gamma_R + \Gamma_i}, \tag{C2b}$$

$$I_Q^P = \sum_{i=L,R} \frac{(E_0 - \mu_P)\Gamma_i\Gamma_R[f_P(E_0) - f_i(E_0)]}{\Gamma_P + \Gamma_i}, \tag{C2c}$$

respectively. Particle conservation implies that $I_p^L + I_p^R + I_p^P = 0$, while energy conservation requires $I_Q^L + \mu_L I_p^L + I_Q^R + \mu_R I_p^R + I_Q^P + \mu_P I_p^P = 0$ [2].

Considering energy and particle conservation, entropy production is given by a specific form,

$$T_L \frac{dS}{dt} = I_p^R A_p^R + I_p^P A_p^P + I_Q^R A_Q^R + I_Q^P A_Q^P, \tag{C3}$$

where $A_p^R = \mu_R - \mu_L$, $A_p^P = \mu_P - \mu_L$, $A_Q^R = 1 - \frac{T_L}{T_R}$, and $A_Q^P = 1 - \frac{T_L}{T_P}$.

The power done by the reservoirs to the system is given by

$$\dot{W} = A_p^R I_p^R + A_p^P I_p^P, \tag{C4}$$

and in the single QD three-terminal systems, we set

$$T_R < T_L < T_P, \tag{C5}$$

and we choose the temperature of the left reservoir as the reference temperature. The efficiency in six different operational

TABLE III. Functionality of a three-terminal single-QD thermal machine.

Thermal progresses	Work and heat currents	Efficiency
Heat engine	$I_Q^R < 0, I_Q^P > 0, \dot{W} < 0$	$\phi_{\rm E} = \frac{-\dot{W}}{I_Q^R A_Q^R + I_Q^P A_Q^P}$
Heat pump	$I_Q^P < 0, I_Q^R < 0, \dot{W} > 0$	$\phi_{\rm P} = \frac{-I_Q^P A_Q^P}{I_Q^R A_Q^R + \dot{W}}$
Refrigerator	$I_Q^R > 0, I_Q^P > 0, \dot{W} > 0$	$\phi_{\rm R} = \frac{-I_Q^R A_Q^R}{I_Q^P A_Q^P + \dot{W}}$
Refrigerator and pump	$I_Q^R > 0, I_Q^P < 0, \dot{W} > 0$	$\phi_{\rm PR} = \frac{-I_Q^R A_Q^R - I_Q^P A_Q^P}{\dot{W}}$
Engine and refrigerator	$I_Q^R > 0, I_Q^P > 0, \dot{W} < 0$	$\phi_{\rm ER} = \frac{-I_Q^R A_Q^R - \dot{W}}{I_Q^P A_Q^P}$
Engine and pump	$I_Q^R < 0, I_Q^P < 0, \dot{W} < 0$	$\phi_{\rm EP} = \frac{-I_Q^P A_Q^P - \dot{W}}{I_Q^R A_Q^P}$

regimes is shown in Table III. In Fig. 6(b), we see that the device with three electronic reservoirs can also perform useful multitasks through adjusting the QD energy E_0 and chemical potential μ_L.

[1] B. Sothmann, R. Sánchez, and A. N Jordan, Thermoelectric energy harvesting with quantum dots, Nanotechnology **26**, 032001 (2015).

[2] J.-H. Jiang and Y. Imry, Linear and nonlinear mesoscopic thermoelectric transport with coupling with heat baths, C. R. Phys. **17**, 1047 (2016).

[3] G. Benenti, G. Casati, K. Saito, and R. S. Whitney, Fundamental aspects of steady-state conversion of heat to work at the nanoscale, Phys. Rep. **694**, 1 (2017).

[4] J. P. Pekola and B. Karimi, Colloquium: Quantum heat transport in condensed matter systems, Rev. Mod. Phys. **93**, 041001 (2021).

[5] R. Wang, C. Wang, J. Lu, and J.-H. Jiang, Inelastic thermoelectric transport and fluctuations in mesoscopic systems, Adv. Phys.: X **7**, 2082317 (2022).

[6] V. Mukherjee and U. Divakaran, Many-body quantum thermal machines, J. Phys.: Condens. Matter **33**, 454001 (2021).

[7] R. S. Whitney, Most Efficient Quantum Thermoelectric at Finite Power Output, Phys. Rev. Lett. **112**, 130601 (2014).

[8] R. S. Whitney, Finding the quantum thermoelectric with maximal efficiency and minimal entropy production at given power output, Phys. Rev. B **91**, 115425 (2015).

[9] V. S. Khrapai, S. Ludwig, J. P. Kotthaus, H. P. Tranitz, and W. Wegscheider, Double-Dot Quantum Ratchet Driven by an Independently Biased Quantum Point Contact, Phys. Rev. Lett. **97**, 176803 (2006).

[10] V. S. Khrapai, S. Ludwig, J. P. Kotthaus, H. P. Tranitz, and W. Wegscheider, Counterflow of Electrons in Two Isolated Quantum Point Contacts, Phys. Rev. Lett. **99**, 096803 (2007).

[11] R. Scheibner, E. G. Novik, T. Borzenko, M. König, D. Reuter, A. D. Wieck, H. Buhmann, and L. W. Molenkamp, Sequential and cotunneling behavior in the temperature-dependent thermopower of few-electron quantum dots, Phys. Rev. B **75**, 041301(R) (2007).

[12] J. R. Prance, C. G. Smith, J. P. Griffiths, S. J. Chorley, D. Anderson, G. A. C. Jones, I. Farrer, and D. A. Ritchie, Electronic Refrigeration of a Two-Dimensional Electron Gas, Phys. Rev. Lett. **102**, 146602 (2009).

[13] H. Thierschmann, M. Henke, J. Knorr, L. Maier, C. Heyn, W. Hansen, H. Buhmann, and L. W. Molenkamp, Diffusion thermopower of a serial double quantum dot, New J. Phys. **15**, 123010 (2013).

[14] J. V. Koski, A. Kutvonen, I. M. Khaymovich, T. Ala-Nissila, and J. P. Pekola, On-Chip Maxwell's Demon as an Information-Powered Refrigerator, Phys. Rev. Lett. **115**, 260602 (2015).

[15] F. Hartmann, P. Pfeffer, S. Höfling, M. Kamp, and L. Worschech, Voltage Fluctuation to Current Converter with Coulomb-Coupled Quantum Dots, Phys. Rev. Lett. **114**, 146805 (2015).

[16] H. Thierschmann, R. Sánchez, B. Sothmann, F. Arnold, C. Heyn, W. Hansen, H. Buhmann, and L. W. Molenkamp, Three-terminal energy harvester with coupled quantum dots, Nat. Nanotechnol. **10**, 854 (2015).

[17] B. Roche, P. Roulleau, T. Jullien, Y. Jompol, I. Farrer, D. A. Ritchie, and D. Glattli, Harvesting dissipated energy with a mesoscopic ratchet, Nat. Commun. **6**, 6738 (2015).

[18] M. Josefsson, A. Svilans, A. M Burke, E. A Hoffmann, S. Fahlvik, C. Thelander, M. Leijnse, and H. Linke, A quantum-dot heat engine operating close to the thermodynamic efficiency limits, Nat. Nanotechnol. **13**, 920 (2018).

[19] M. Josefsson, A. Svilans, H. Linke, and M. Leijnse, Optimal power and efficiency of single quantum dot heat engines: Theory and experiment, Phys. Rev. B **99**, 235432 (2019).

[20] Y. Kleeorin, H. Thierschmann, H. Buhmann, A. Georges, L. Molenkamp, and Y. Meir, How to measure the entropy of a mesoscopic system via thermoelectric transport, Nat. Commun. **10**, 5801 (2019).

[21] G. Jaliel, R. K. Puddy, R. Sánchez, A. N. Jordan, B. Sothmann, I. Farrer, J. P. Griffiths, D. A. Ritchie, and C. G. Smith, Experimental Realization of a Quantum Dot Energy Harvester, Phys. Rev. Lett. **123**, 117701 (2019).

[22] S. Dorsch, A. Svilans, M. Josefsson, B. Goldozian, M. Kumar, C. Thelander, A. Wacker, and A. Burke, Heat driven transport in serial double quantum dot devices, Nano Lett. **21**, 988 (2021).

[23] B. Dutta, D. Majidi, N. W. Talarico, N. Lo Gullo, H. Courtois, and C. B. Winkelmann, Single-Quantum-Dot Heat Valve, Phys. Rev. Lett. **125**, 237701 (2020).

[24] R.-X. Zhai, F.-M. Cui, Y.-H. Ma, C. P. Sun, and H. Dong, Experimental implementation of finite-time carnot cycle, arXiv:2206.10153 (2022)

[25] P. Pietzonka and U. Seifert, Universal Trade-Off between Power, Efficiency, and Constancy in Steady-State Heat Engines, Phys. Rev. Lett. **120**, 190602 (2018).

[26] Y.-Q. Liu, D.-H. Yu, and C.-S. Yu, Common environmental effects on quantum thermal transistor, Entropy **24**, 32 (2022).

[27] G. D. Mahan and J. O. Sofo, The best thermoelectric, Proc. Natl. Acad. Sci. USA **93**, 7436 (1996).

[28] J. Zhou, R. Yang, G. Chen, and M. S. Dresselhaus, Optimal Bandwidth for High Efficiency Thermoelectrics, Phys. Rev. Lett. **107**, 226601 (2011).

[29] F. Mazza, S. Valentini, R. Bosisio, G. Benenti, V. Giovannetti, R. Fazio, and F. Taddei, Separation of heat and charge currents for boosted thermoelectric conversion, Phys. Rev. B **91**, 245435 (2015).

[30] O. Entin-Wohlman, Y. Imry, and A. Aharony, Three-terminal thermoelectric transport through a molecular junction, Phys. Rev. B **82**, 115314 (2010).

[31] D. Sánchez and R. López, Scattering Theory of Nonlinear Thermoelectric Transport, Phys. Rev. Lett. **110**, 026804 (2013).

[32] J.-H. Jiang, O. Entin-Wohlman, and Y. Imry, Three-terminal semiconductor junction thermoelectric devices: improving performance, New J. Phys. **15**, 075021 (2013).

[33] B. Sothmann, R. Sánchez, A. N Jordan, and M. Büttiker, Powerful energy harvester based on resonant-tunneling quantum wells, New J. Phys. **15**, 095021 (2013).

[34] K. Yamamoto, O. Entin-Wohlman, A. Aharony, and N. Hatano, Efficiency bounds on thermoelectric transport in magnetic fields: The role of inelastic processes, Phys. Rev. B **94**, 121402(R) (2016).

[35] Y. Zhang, G. Lin, and J. Chen, Three-terminal quantum-dot refrigerators, Phys. Rev. E **91**, 052118 (2015).

[36] L. Wang, Z. Wang, C. Wang, and J. Ren, Cycle Flux Ranking of Network Analysis in Quantum Thermal Devices, Phys. Rev. Lett. **128**, 067701 (2022).

[37] R. Sánchez and M. Büttiker, Optimal energy quanta to current conversion, Phys. Rev. B **83**, 085428 (2011).

[38] H. Thierschmann, F. Arnold, M. Mittermüller, L. Maier, C. Heyn, W. Hansen, H. Buhmann, and L. W. Molenkamp, Thermal gating of charge currents with coulomb coupled quantum dots, New J. Phys. **17**, 113003 (2015).

[39] S. M. Tabatabaei, D. Sánchez, Alfredo L. Yeyati, and R. Sánchez, Andreev-Coulomb Drag in Coupled Quantum Dots, Phys. Rev. Lett. **125**, 247701 (2020).

[40] J.-H. Jiang, O. Entin-Wohlman, and Y. Imry, Thermoelectric three-terminal hopping transport through one-dimensional nanosystems, Phys. Rev. B **85**, 075412 (2012).

[41] B. Cleuren, B. Rutten, and C. Van den Broeck, Cooling by Heating: Refrigeration Powered by Photons, Phys. Rev. Lett. **108**, 120603 (2012).

[42] J. Lu, R. Wang, J. Ren, M. Kulkarni, and J.-H. Jiang, Quantum-dot circuit-qed thermoelectric diodes and transistors, Phys. Rev. B **99**, 035129 (2019).

[43] R. Kosloff and A. Levy, Quantum heat engines and refrigerators: Continuous devices, Annu. Rev. Phys. Chem. **65**, 365 (2014).

[44] A. Mani and C. Benjamin, Helical thermoelectrics and refrigeration, Phys. Rev. E **97**, 022114 (2018).

[45] D. Sánchez, R. Sánchez, R. López, and B. Sothmann, Nonlinear chiral refrigerators, Phys. Rev. B **99**, 245304 (2019).

[46] J. Ren, P. Hänggi, and B. Li, Berry-Phase-Induced Heat Pumping and Its Impact on the Fluctuation Theorem, Phys. Rev. Lett. **104**, 170601 (2010).

[47] Z. Wang, L. Wang, J. Chen, C. Wang, and J. Ren, Geometric heat pump: Controlling thermal transport with time-dependent modulations, Front. Phys. **17**, 1 (2022).

[48] Z. Wang, J. Chen, and J. Ren, Geometric heat pump and no-go restrictions of nonreciprocity in modulated thermal diffusion, Phys. Rev. E **106**, L032102 (2022).

[49] G. Manzano and R. Zambrini, Quantum thermodynamics under continuous monitoring: A general framework, AVS Quantum Sci. **4**, 025302 (2022).

[50] Z.-C. Tu, Abstract models for heat engines, Front. Phys. **16**, 33202 (2021).

[51] J.-H. Jiang and Y. Imry, Enhancing Thermoelectric Performance Using Nonlinear Transport Effects, Phys. Rev. Appl. **7**, 064001 (2017).

[52] J.-H. Jiang and Y. Imry, Near-field three-terminal thermoelectric heat engine, Phys. Rev. B **97**, 125422 (2018).

[53] O. Entin-Wohlman, Y. Imry, and A. Aharony, Enhanced performance of joint cooling and energy production, Phys. Rev. B **91**, 054302 (2015).

[54] G. Manzano, R. Sánchez, R. Silva, G. Haack, J. B. Brask, N. Brunner, and P. P. Potts, Hybrid thermal machines: Generalized thermodynamic resources for multitasking, Phys. Rev. Res. **2**, 043302 (2020).

[55] G. T. Landi and M. Paternostro, Irreversible entropy production: From classical to quantum, Rev. Mod. Phys. **93**, 035008 (2021).

[56] K. Hammam, H. Leitch, Y. Hassouni, and G. De Chiara, Exploiting coherence for quantum thermodynamic advantage, New J. Phys. **24**, 113053 (2022).

[57] T. V. Marcella, Entropy production and the second law of thermodynamics: An introduction to second law analysis, Am. J. Phys. **60**, 888 (1992).

[58] S. Mukherjee, B. De, and B. Muralidharan, Three-terminal vibron-coupled hybrid quantum dot thermoelectric refrigeration, J. Appl. Phys. **128**, 234303 (2020).

[59] F. Hajiloo, R. Sánchez, R. S. Whitney, and J. Splettstoesser, Quantifying nonequilibrium thermodynamic operations in a multiterminal mesoscopic system, Phys. Rev. B **102**, 155405 (2020).

[60] M. Carrega, L. M. Cangemi, G. De Filippis, V. Cataudella, G. Benenti, and M. Sassetti, Engineering dynamical couplings for quantum thermodynamic tasks, PRX Quantum **3**, 010323 (2022).

[61] P. Strasberg and A. Winter, First and second law of quantum thermodynamics: A consistent derivation based on a microscopic definition of entropy, PRX Quantum **2**, 030202 (2021).

[62] J.-H. Jiang, Thermodynamic bounds and general properties of optimal efficiency and power in linear responses, Phys. Rev. E **90**, 042126 (2014).

[63] G. J. Snyder and T. S. Ursell, Thermoelectric Efficiency and Compatibility, Phys. Rev. Lett. **91**, 148301 (2003).

[64] Y.-Y. Liu, K. D. Petersson, J. Stehlik, J. M. Taylor, and J. R. Petta, Photon Emission from a Cavity-Coupled Double Quantum Dot, Phys. Rev. Lett. **113**, 036801 (2014).

[65] M. J. Gullans, Y.-Y. Liu, J. Stehlik, J. R. Petta, and J. M. Taylor, Phonon-Assisted Gain in a Semiconductor Double Quantum Dot Maser, Phys. Rev. Lett. **114**, 196802 (2015).

[66] J. Lu, R. Wang, C. Wang, and J.-H. Jiang, Brownian thermal transistors and refrigerators in mesoscopic systems, Phys. Rev. B **102**, 125405 (2020).

[67] G. Chen, *Nanoscale Energy Transport and Conversion* (Oxford University Press, London, 2005).

[68] A. Miller and E. Abrahams, Impurity conduction at low concentrations, Phys. Rev. **120**, 745 (1960).

[69] Y. Meir and N. S. Wingreen, Landauer Formula for the Current Through an Interacting Electron Region, Phys. Rev. Lett. **68**, 2512 (1992).

[70] S. Datta, *Electronic Transport in Mesoscopic Systems* (Cambridge University Press, Cambridge, UK, 1995).

[71] M. Esposito, K. Lindenberg, and C. Van den Broeck, Thermoelectric efficiency at maximum power in a quantum dot, Europhys. Lett. **85**, 60010 (2009).

[72] O. Kedem and S. R. Caplan, Degree of coupling and its relation to efficiency of energy conversion, Trans. Faraday Soc. **61**, 1897 (1965).

[73] S. Saryal, M. Gerry, I. Khait, D. Segal, and B. K. Agarwalla, Universal Bounds on Fluctuations in Continuous Thermal Machines, Phys. Rev. Lett. **127**, 190603 (2021).

[74] V. Holubec and A. Ryabov, Cycling Tames Power Fluctuations near Optimum Efficiency, Phys. Rev. Lett. **121**, 120601 (2018).

[75] C. Van den Broeck, Thermodynamic Efficiency at Maximum Power, Phys. Rev. Lett. **95**, 190602 (2005).

[76] K. Proesmans, B. Cleuren, and C. Van den Broeck, Power-Efficiency-Dissipation Relations in Linear Thermodynamics, Phys. Rev. Lett. **116**, 220601 (2016).

[77] N. Shiraishi, K. Saito, and H. Tasaki, Universal Trade-Off Relation between Power and Efficiency for Heat Engines, Phys. Rev. Lett. **117**, 190601 (2016).

[78] J. Lu, Y. Liu, R. Wang, C. Wang, and J.-H. Jiang, Optimal efficiency and power, and their trade-off in three-terminal quantum thermoelectric engines with two output electric currents, Phys. Rev. B **100**, 115438 (2019).

[79] J.-H. Jiang, Enhancing efficiency and power of quantum-dots resonant tunneling thermoelectrics in three-terminal geometry by cooperative effects, J. Appl. Phys. **116**, 194303 (2014).

[80] J. Lu, R. Wang, Y. Liu, and J.-H. Jiang, Thermoelectric cooperative effect in three-terminal elastic transport through a quantum dot, J. Appl. Phys. **122**, 044301 (2017).

[81] T. Krause, G. Schaller, and T. Brandes, Incomplete current fluctuation theorems for a four-terminal model, Phys. Rev. B **84**, 195113 (2011).

[82] D. Venturelli, R. Fazio, and V. Giovannetti, Minimal Self-Contained Quantum Refrigeration Machine Based on Four Quantum Dots, Phys. Rev. Lett. **110**, 256801 (2013).

[83] J. Matthews, F. Battista, D. Sánchez, P. Samuelsson, and H. Linke, Experimental verification of reciprocity relations in quantum thermoelectric transport, Phys. Rev. B **90**, 165428 (2014).

[84] C. Bergenfeldt, P. Samuelsson, B. Sothmann, C. Flindt, and M. Büttiker, Hybrid Microwave-Cavity Heat Engine, Phys. Rev. Lett. **112**, 076803 (2014).

[85] P. P. Hofer and B. Sothmann, Quantum heat engines based on electronic mach-zehnder interferometers, Phys. Rev. B **91**, 195406 (2015).

[86] J.-T. Lü, J.-S. Wang, P. Hedegård, and M. Brandbyge, Electron and phonon drag in thermoelectric transport through coherent molecular conductors, Phys. Rev. B **93**, 205404 (2016).

[87] B. Bhandari, G. Chiriacò, P. A. Erdman, R. Fazio, and F. Taddei, Thermal drag in electronic conductors, Phys. Rev. B **98**, 035415 (2018).

[88] K. Brandner, T. Hanazato, and K. Saito, Thermodynamic Bounds on Precision in Ballistic Multiterminal Transport, Phys. Rev. Lett. **120**, 090601 (2018).

[89] R. Sánchez, P. Samuelsson, and P. P. Potts, Autonomous conversion of information to work in quantum dots, Phys. Rev. Res. **1**, 033066 (2019).

[90] K. Hammam, Y. Hassouni, R. Fazio, and G. Manzano, Optimizing autonomous thermal machines powered by energetic coherence, New J. Phys. **23**, 043024 (2021).

[91] S. Takada, G. Georgiou, E. Arrighi, H. Edlbauer, Y. Okazaki, S. Nakamura, A. Ludwig, A. D. Wieck, M. Yamamoto, C. Bäuerle, and N.-H. Kaneko, Heat-driven electron-motion in a nanoscale electronic circuit, J. Phys. Soc. Jpn. **90**, 113707 (2021).

[92] J. Lu, J.-H. Jiang, and Y. Imry, Unconventional four-terminal thermoelectric transport due to inelastic transport: Cooling by transverse heat current, transverse thermoelectric effect, and maxwell demon, Phys. Rev. B **103**, 085429 (2021).

[93] R. S. Whitney, R. Sánchez, F. Haupt, and J. Splettstoesser, Thermoelectricity without absorbing energy from the heat sources, Physica E **75**, 257 (2016).

[94] J.-H. Jiang, M. Kulkarni, D. Segal, and Y. Imry, Phonon thermoelectric transistors and rectifiers, Phys. Rev. B **92**, 045309 (2015).

[95] W. Niedenzu and G. Kurizki, Cooperative many-body enhancement of quantum thermal machine power, New J. Phys. **20**, 113038 (2018).